Permanent Magnet Vernier Generator Design for a Small-scale Passive Wind Generator System

C.J.J. Labuschagne, *Student Member, IEEE,* M.J. Kamper, *Senior Member, IEEE,*
Department of Electrical & Electronic Engineering
Stellenbosch University
Stellenbosch, South Africa
17539455@sun.ac.za, kamper@sun.ac.za

2021 IEEE International Electric Machines & Drives Conference (IEMDC) | 978-1-6654-0510-2/21/$31.00 ©2021 IEEE | DOI: 10.1109/IEMDC47953.2021.9449547

***Abstract*—In this paper it is proposed that permanent magnet vernier generators be used in a small-scale passive wind generator system. Various aspects such as the machine selection, design optimisation, torque quality and the overall feasibility of the proposal are investigated. The performance and power matching results that are obtained for the permanent magnet vernier generator with a magnetic gearing ratio of eight are very attractive for this application. Only the vernier generator with a magnetic gearing ratio of five is not suited for this application due to poor torque quality. Designs are confirmed by comparing 2D and 3D finite element results.**

***Index Terms*—passive wind generator system, permanent magnet vernier generator, small-scale wind turbine**

I. Introduction

Permanent magnet vernier machines (PMVM) are very much at the forefront of current research on alternative wind generator technologies, with power levels ranging from small- to large-scale applications [1] [2]. The extensive review on PMVMs in [3] highlights that PMVMs are paricularly suited for low speed direct-drive applications and have the potential for a high torque density. The PMVM's torque producing capability is especially attractive for wind generator technology. However, the practicality of PMVMs for industry are hindered by their characteristic of poor power factors. This can predominantly be attributed to the excessive leakage flux in PMVMs and to inherently high operating frequencies due to machine selection, with both factors contributing to a large reactance. Complex design structures have been proposed to improve the PMVM's power factor [4] [5], but from a manufacturing perspective these proposals are not always ideal.

In this paper it is proposed that PMVMs be used in small-scale (< 20 kW) passive wind generator systems, such as the one shown in Fig. 1. For this application the PMVM's large internal reactance is not considered to be a drawback (explanation given in Section II). For the passive system in Fig. 1, the generator is uncontrolled and is only connected via a diode bridge rectifier to the system's battery storage. As of yet, the design of a PM vernier generator (PMVG) for such an uncontrolled passive wind generator system has not been done. In this paper, the design approach for PMVGs, used in a passive wind generator system, is formulated according to the system's specifications. The design results are then evaluated; focussing on the wind generators' power matching with the wind turbine, generator performance and generator torque quality. The aim of the investigation is to determine whether the proposal is feasible and whether using PMVGs offer any advantage for this application.

This work was financially supported by the Centre for Renewable and Sustainable Energy Studies at the Stellenbosch University, Stellenbosch, South Africa and the National Research Foundation in South Africa.

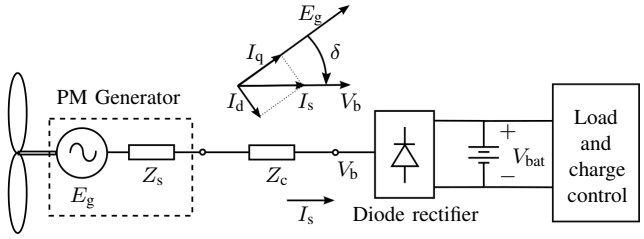

Fig. 1. Single line diagram of a passive wind energy system with uncontrolled diode rectifier and battery storage.

Furthermore, small-scale wind generator systems are ideal for energy generation in either ac- or dc-microgrids and there are current incentives to make small-scale wind generator systems more cost effective [6]. The passive system in Fig. 1 is especially attractive for remote communities and developing countries. Minimal power electronics are used in the passive system. The passive system is therefore potentially more reliable and cost effective, since the power electronics in small-scale wind generator systems are the components most prone to failure [7]. The preferred generator technology in small-scale wind generator systems are PM synchronous generators (PMSG), but the torque producing capability of PMVGs may further reduce generator cost and mass. This was shown in the direct comparison between a PMSG and PMVG for a small-scale *actively controlled* wind generator system in [8]. However, the compromise for the larger inverter due to the PMVG's power factor is still the levelling trade-off. This, then serves as further motivation for the investigation done in this paper, i.e. using PMVGs in small-scale uncontrolled passive wind generator systems.

II. Impedance Matching in Passive Wind Generator Systems

The PMVG design in this paper is for a sub 5 kW passive wind generator system. The specifications and desired operat-

978-1-6654-0510-2/21/$31.00 ©2021 IEEE

Authorized licensed use limited to: University of Stellenbosch. Downloaded on June 16,2021 at 11:45:02 UTC from IEEE Xplore. Restrictions apply.

TABLE I
SUMMARY OF SPECIFIED OPERATING POINTS.

	n_c	n_r
Wind speed	3 m/s	12 m/s
Turbine speed	110 r/min	320 r/min
Generated power, P_g	0 kW	4.2 kW
Battery/dc grid voltage, V_b	48 V	

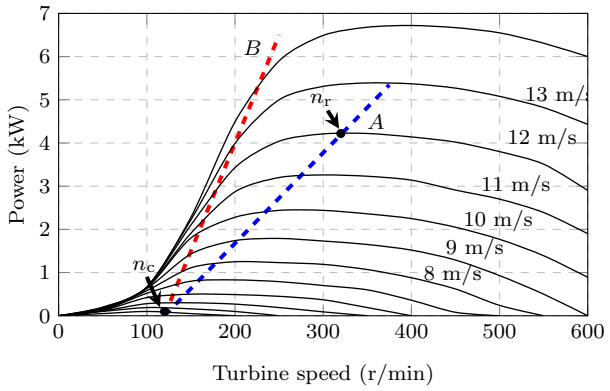

Fig. 2. Wind turbine power versus speed curves.

ing points are summarised in Table I, where n_c is the cut-in speed and n_r is the rated operating speed. The wind turbine's power versus speed curves are shown in Fig. 2. Because it is an uncontrolled passive system, the internal impedance of the generator, Z_s in Fig. 1, needs to match correctly with the load voltage of the battery storage. This then ensures that the generated power matches with the available wind turbine power at the rated operating point, n_r. The example power curve *A*, in Fig. 2, shows the desired power matching for the passive system. Designing a conventional PMSG for such a natural impedance matching is possible, but requires alterations to the machine geometry in order to significantly increase the PMSG's impedance (reactance) [9].

Consider the following estimation for the required reactance: The phasor diagram for the passive system, that is shown in Fig. 3, can be derived from the equivalent *dq*-circuit modelling of the PM generator in Fig. 1. In Fig. 3, the constrained terminal voltage, V_b, is the fixed fundamental per phase voltage on the ac-side of the diode rectifier. The system will operate at a unity displacement power factor [10], i.e. I_s and V_b are in phase. At rated power, E_g can be calculated using

$$E_g = aV_b = \frac{n_r}{n_c}V_b. \tag{1}$$

For simplification, it is further assumed that the resistance R_{st} in Fig. 3 is negligible. Subsequently, from Fig. 3, we have

$$\cos(\delta) = \frac{V_b}{E_g} = \frac{1}{a} \Rightarrow \delta = \cos^{-1}\left(\frac{1}{a}\right) \tag{2}$$

and

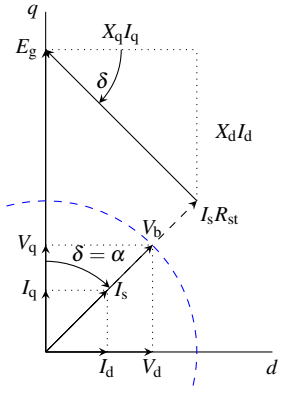

Fig. 3. Passive system phasor diagram.

TABLE II
PREDICTED *dq* VALUES AT RATED POWER ($n_r = 2.91$ pu).

$P_g = 1.0$ pu	$V_b = 1.0$ pu	$I_s = 1.0$ pu	$E_g = 2.91$ pu
$V_d = 0.94$ pu	$I_d = 0.94$ pu		$X_d = 2.73$ pu
$V_q = 0.344$ pu	$I_q = 0.344$ pu		$X_q = 2.73$ pu

$$\tan(\delta) = \frac{V_d}{V_q} = \frac{I_d}{I_q} = \frac{X_dI_d}{X_qI_q} \Rightarrow \frac{X_d}{X_q} = 1. \tag{3}$$

Substituting $a = 2.91$, obtained from Table I, into (2) and then δ into (3) we have (4). With $V_b = I_s = 1$ pu, the calculated per unit values at rated power are summarised in Table II.

$$\frac{I_d}{I_q} = \tan(68^\circ) = 2.73 \tag{4}$$

Of course, R_{st} in Fig. 3 cannot be ignored. Nonetheless, the approximated per unit reactance in Table II gives perspective on how high the reactance must be to have the desired power matching. The required reactance at *base speed* is $X_d = X_q = 2.73/2.91 = 0.94$ pu, whereas surface mount PMSGs with non-overlapping windings typically have reactance values between 0.2 and 0.4 pu. An example of the power matching, where the generator's internal reactance is too low, is shown in Fig. 2, power curve *B*.

From the above estimation for the required generator impedance, it becomes more evident why the naturally high reactance of PMVGs is not considered to be a drawback for this application and might compliment the passive wind generator system.

III. PM VERNIER MACHINES

The vernier machine's potential for a higher torque density is due to the fact that vernier machines have two torque producing components, as opposed to conventional machines that only have one. The two torque producing components are the result of "harmonic coupling" taking place; i.e. between the PM rotor's working harmonic and a higher order

Authorized licensed use limited to: University of Stellenbosch. Downloaded on June 16,2021 at 11:45:02 UTC from IEEE Xplore. Restrictions apply.

TABLE III
VERNIER MACHINE SELECTION WITH IMPOSED FREQUENCY CONSTRAINT AT RATED SPEED, n_r.

G_r	5			8			11			14		
p_s	Q_s	p_r	f_e (Hz)	Q_s	p_r	f_e (Hz)	Q_s	p_r	f_e (Hz)	Q_s	p_r	f_e (Hz)
1	6	5	26.67	9	8	42.67	12	11	58.67	15	14	74.67
2	12	10	53.33	18	16	85.53	24	22	117.33	30	28	149.33
3	18	15	80.0	27	24	128.0	36	33	176.0	45	42	224.0
4	24	20	106.67	36	32	170.67	48	44	234.67	60	56	298.67
5	30	25	133.33	45	40	213.33	60	55	293.33	75	70	373.33
q	1			1.5			2			2.5		

stator winding-MMF harmonic, as well as the resulting flux-modulated harmonic with the fundamental stator winding-MMF harmonic [11]. Therefore, the vernier machine selection is subject to the relationship given by

$$p_s = Q_s \pm p_r \Rightarrow p_s = Q_s - p_r, \tag{5}$$

where p_s is the number of stator pole pairs, Q_s is the number of flux-modulating poles and p_r is the number of rotor PM pole pairs.

The ratio of the number of rotor- to stator pole pairs, G_r, is referred to as the harmonic coupling factor or the magnetic gearing ratio:

$$G_r = \frac{p_r}{p_s} \tag{6}$$

Equations for the generated torque and synchronous reactance, obtained from [8], are given in (7) and (8) respectively. The gearing ratio of (6) is present in both (7) and (8) and highlights the fundamental trade-off for vernier machine selection: a larger G_r results in a better torque producing capability, but at the potential cost of a poorer power factor.

$$T_g = K_w N_s I_s d_{air} l_{fe} \left[B_{PM0} + \frac{p_r}{p_s} \frac{B_{PM1}}{2} \right] \tag{7}$$

$$X_i = \omega_r p_r L_i = \omega_r \frac{p_r}{p_s} \frac{m}{2} \frac{\pi \mu_0 N_s^2 l_{fe} d_{air}}{4 p_s g} K_w \tag{8}$$

The two main vernier machine topologies are the conventional topology with overlapping windings and the split-tooth topology with non-overlapping windings. Only the conventional topology's design is done in this paper. In the case of the conventional topology, the stator teeth act as the flux-modulating poles. Using (5) and (6), the possible PMVG slot-pole combinations are summarised in Table III. For small-scale wind generator systems, the wind generator needs to overcome both generator cogging torque and open-circuit losses (predominantly core losses) up to the system's cut-in speed, n_c, to start generating power. Core losses increase with an increase in electrical frequency. Therefore, a maximum allowed electrical frequency of $f_e = 130$ Hz at the rated operating speed is imposed on the machine selection. This constraint is indicated in Table III. The three selected PMVG's, with $G_r = 5, 8$ and 11 respectively, are indicated with a darker highlight. These machine selections are at the maximum frequency constraint and also have a realistic number of stator slots for manufacturing the stator winding.

IV. DESIGN OPTIMISATION METHODOLOGY

Using a multi-objective optimisation algorithm in the design process is inevitable. The PMVGs need to be designed with the correct reactance to achieve the desired impedance matching with the turbine (Section II), while taking the other objectives and constraints into account. For the design optimisation, the NSGA-II algorithm [12] is used and PMVG solutions are done using static finite element analysis (FEA).

The multi-objective function, for the PMVG design optimisation, is given by

$$\min_{\mathbf{X}} \ \mathbf{F}(\mathbf{X}) = \min_{\mathbf{X}} \begin{bmatrix} M_{PM}(\mathbf{X}) \\ M_{active}(\mathbf{X}) \\ Z_{error} \end{bmatrix}. \tag{9}$$

Minimising the PMVG's active mass, M_{active}, and PM mass, M_{PM}, is of interest, as this effectively reduces generator- and system costs. The active mass is calculated as

$$M_{active} = M_{fe} + M_{PM} + M_{cu}, \tag{10}$$

where M_{fe} is the collective mass of the stator- and rotor-iron laminations, and M_{cu} is the total copper mass, which includes the end-winding copper mass. The other objective in (9) is to minimise the impedance error, Z_{error}. This is the required

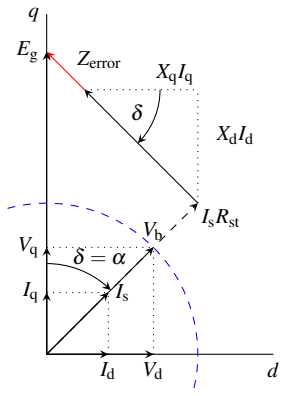

Fig. 4. The impedance error, Z_{error}, that needs to be minimised in the objective function given in (9). ($Z_{error} = X_{error}$)

Authorized licensed use limited to: University of Stellenbosch. Downloaded on June 16,2021 at 11:45:02 UTC from IEEE Xplore. Restrictions apply.

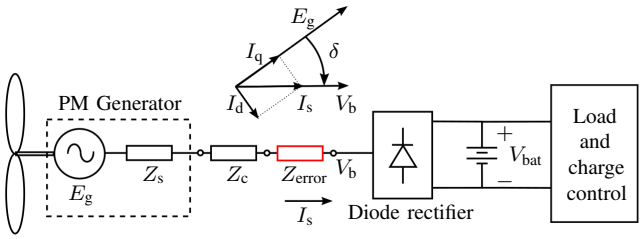

Fig. 5. Single-line diagram of PM wind generator with external inductance for impedance matching connected in passive wind turbine system.

difference in generator impedance, if not zero, to match the generator's power with the turbine at the rated operating point as shown in Fig. 4. The impedance error is calculated with the solution method for external impedance matching given in [13]. The impedance error is visually illustrated in Fig. 5, as a physical external impedance component that is added to the passive generator system between the generator and the diode bridge rectifier. The impedance error is given as feedback to the optimisation algorithm and ensures that the optimisation algorithm finds non-dominated PMVG solutions where $Z_{\text{error}} \approx 0$, since any significant deviation from this will result in undesired power matching. This way, the PMVGs are designed for the correct synchronous impedance Z_s.

The PMVG solutions in the design optimisation are subject to the design constraints at the rated operating point, given by

$$\mathbf{U} = \begin{bmatrix} P_g \\ \eta \\ J_{\text{rms}} \\ \overline{\tau_r} \end{bmatrix} = \begin{bmatrix} 4.2 \text{ kW} \\ \geq 90\% \\ \leq 5 \text{ A/mm}^2 \\ \geq 2.2 \end{bmatrix}. \tag{11}$$

In (11), P_g is the rated power, η is the generator efficiency, J_{rms} the maximum allowed RMS current density and $\overline{\tau_r}$ is the normalised pole pitch. The effect of the air gap length on the electromagnetic performance of surface mount PMVMs was investigated in [14], wherein $\overline{\tau_r}$ is defined as

$$\overline{\tau_r} = \frac{\tau_r}{g + \frac{h_m}{\mu_r}}. \tag{12}$$

In (12), τ_r is the rotor pole pitch, g is the mechanical air gap's height, h_m is the PM height and μ_r is the PM's relative permeability. For a PMVG rated at 3 kW it was found in [14] that when $\overline{\tau_r} > 2.2$, the PMVG achieves a higher torque density than a conventional PMSG. Since the power level for this investigation is at 4.2 kW (close to 3 kW) and there is no direct comparison done between PMVGs and conventional PMSGs in this paper, $\overline{\tau_r} > 2.2$ is added as an additional constraint for the design optimisation in (11).

The dimensional array

$$\mathbf{X} = \begin{bmatrix} d_o & h_{yr} & h_m & \theta_m & \theta_{so} & h_t & h_s & w_s & h_{ys} & l_{fe} \end{bmatrix}^T, \tag{13}$$

with the PMVG's geometrical design variables is given to the design optimisation as input. The variables in (13), are defined

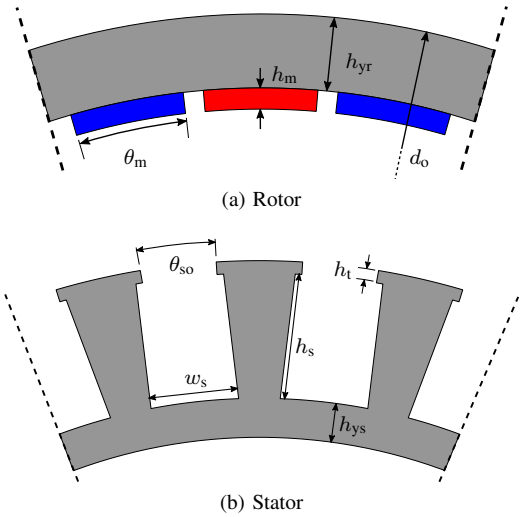

Fig. 6. Vernier machine's geometrical design variables.

in Fig. 6. For all of the PMVG solutions, the height of the mechanical air gap is kept constant at $g = 1$ mm.

V. Results and Discussion

A. Design Optimisation Results

The pareto front solutions for the respective PMVGs, with different magnetic gearing ratios, are given in Fig. 7. The pareto fronts in Fig. 7 give valuable insight in terms of M_{active} and M_{PM}, showing little trade-off between the PMVGs with $G_r = 5$ and $G_r = 8$. It is unexpected that the PMVG with a lower G_r would do slightly better in this regard. However, a similar trend for PMVGs with a higher number of stator pole pairs, p_s, is found in [8].

For the PMVG with $G_r = 11$, the pareto front solutions in Fig. 7 have a greater M_{active} and M_{PM} than the aforementioned PMVGs. On average, the PMVG solutions for $G_r = 11$ have approximately 40% more PM material. Once more, it is unexpected that the PMVGs with a lower G_r would do that much better in terms of both M_{active} and M_{PM}. The pareto front solutions for the PMVG with $G_r = 11$ did converge, however

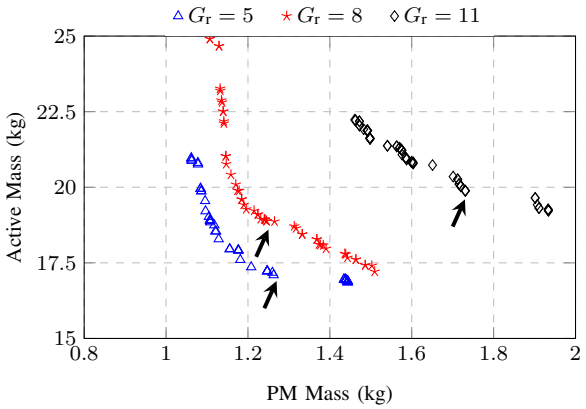

Fig. 7. Pareto front optimisation results ($Z_{\text{error}} = 0$ for all).

Authorized licensed use limited to: University of Stellenbosch. Downloaded on June 16,2021 at 11:45:02 UTC from IEEE Xplore. Restrictions apply.

TABLE IV
COMPARISON OF SELECTED PARETO FRONT SOLUTIONS.

PMVG	$G_r = 5$	$G_r = 8$	$G_r = 11$
p_s	4	3	2
Q_s	24	27	24
p_r	20	24	22
M_{PM} (kg)	1.26	1.23	1.73
M_{active} (kg)	17.09	18.95	19.88
Z_{error}	0.0	0.0	0.0
P_g (kW)	4.10	4.19	4.12
η (%)	91.1	92.4	95.9
J (A/mm^2)	4.94	5.0	1.90
$\overline{\tau_r}$	5.22	4.91	5.83
d_o (mm)	278	314	392
l_{fe} (mm)	77	80	62

the limiting factor in this case is the power constraint, P_g in (11), at the rated operating point. Although a large generator impedance is required for this application, as explained in Section II, the PMVG with $G_r = 11$ is prone to excessive leakage flux and subsequently a larger synchronous reactance, as also stated in Section III. As a result, NSGA-II's elitist search algorithm easily finds PMVG solutions that minimise the impedance matching error for the multi-objective function in (9), with $Z_{error} = 0$ for all of the solutions in Fig. 7, but struggles to find solutions that adhere to the power matching design constraint, P_g, in (11). For all of the $G_r = 11$ pareto front solutions in Fig. 7, none of the other constraints converged at their minimum or maximum allowed values given in (11).

The performance results of the three selected PMVGs indicated in Fig. 7, are summarised in Table IV for evaluation. All of the design constraints are met. It is also evident from observing the results in Table IV that the imposed constraint on the normalised pole pitch, $\overline{\tau_r}$, in the design optimisation is irrelevant for this selection of PMVGs and can be excluded from future PMVG designs for this application.

One more notable result from the pareto fronts in Fig. 7, is that the PMVGs tend to fare better in terms of M_{active} and M_{PM} when compared to the PMSGs designed for this application in [9]. Thus indicating that PMVGs are potentially more cost effective for passive wind generator systems.

B. Power Matching

All of the pareto front solutions in Fig. 7 (and Table IV) have an impedance error of $Z_{error} = 0$, i.e. the PMVGs achieve the desired power matching with the wind turbine. To show that the PMVGs achieve the desired power matching, the respective operating power curves for the PMVGs in Table IV are plotted against the wind turbine power versus speed curves in Fig. 8. It is shown in Fig. 8 that the PMVGs achieve good power matching with the wind turbine at low wind speeds, which is essential for this application, and match with the turbine at the rated operating speed n_r.

The overall performance and power matching results are desirable and no external impedance matching is necessary, i.e. the PMVGs match *naturally* with the wind turbine. The latter is another potential advantage over conventional surface mounted PMSGs, that tend to require an external reactance to be connected to the system [9] in order to achieve the desired power matching with the wind turbine.

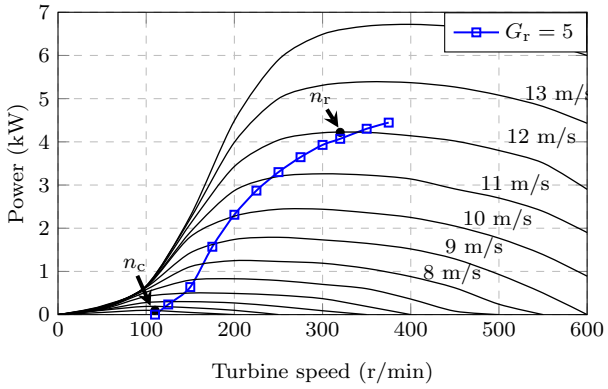

(a)

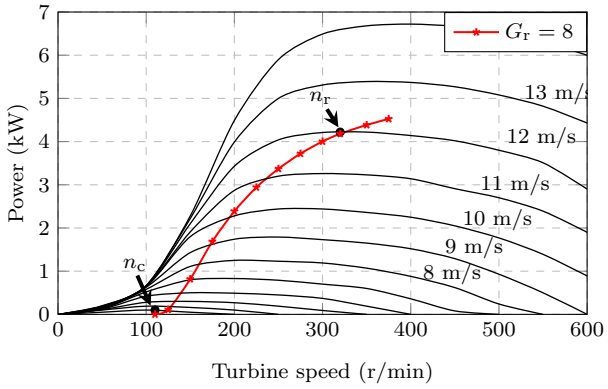

(b)

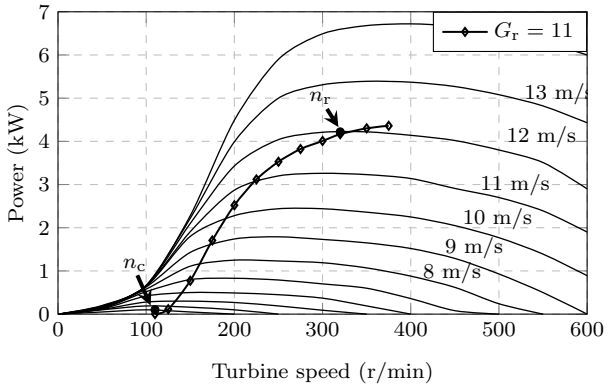

(c)

Fig. 8. Operating power curves of the selected PMVGs.

Authorized licensed use limited to: University of Stellenbosch. Downloaded on June 16,2021 at 11:45:02 UTC from IEEE Xplore. Restrictions apply.

TABLE V
TORQUE QUALITY COMPARISON.

PMVG	$G_r = 5$	$G_r = 8$	$G_r = 11$
ΔT_{cog} (%)	17.9	0.8	5.1
ΔT_r (%)	30.1	0.6	7.8
LCM(Q_s,$2p_r$)	120	432	264

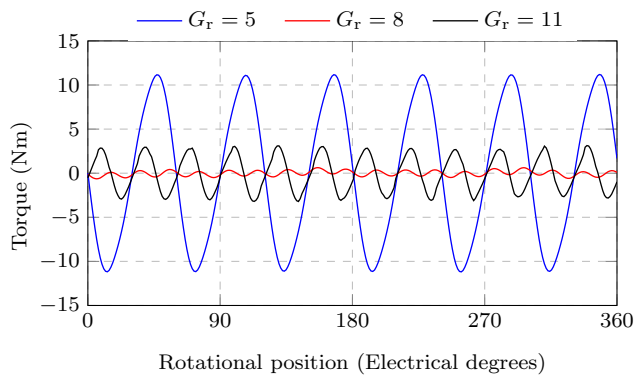

Fig. 9. FE predicted cogging torque, ΔT_{cog}, of the three selected machines.

C. Torque Quality

Low generator cogging torque is essential for small-scale wind turbines, as the wind turbine has to overcome this to start generating power. The cogging torque, ΔT_{cog}, and torque ripple, ΔT_r, results for the respective PMVGs in Table IV, are summarised in Table V. The FE predicted cogging torque of the respective PMVGs, are also shown for the mechanical rotation of one rotor pole pair (360 electrical degrees) in Fig. 9.

The extremely low cogging torque results for the PMVG with $G_r = 8$ in Table V is ideal. The PMVG has almost zero cogging torque and negligible torque ripple at the rated operating point. These results are attractive, because no special design steps were taken to minimise the PMVG's cogging torque. On the other hand, the cogging torque and torque ripple results for the PMVG with $G_r = 5$, indicate that it is unsuited for this application. The high cogging torque for the PMVG with $G_r = 5$ correlates with the designs in [8] and is theoretically expected because of the relatively small least common multiple (LCM) between the stator slots, Q_s, and the PM rotor poles, $2p_r$, [15].

For the PMVG with $G_r = 11$, the cogging torque is still reasonably low and can even be further reduced in the design process. However, in terms of mass, the results in Fig. 7 show that the $G_r = 11$ PMVG is not an option (PMVG with $G_r = 8$ is superior in terms of M_{active} and M_{PM}). Other solutions in Fig. 7, also indicate that the PMVG with $G_r = 11$ is more sensitive to cogging torque; with some of the solutions having a cogging torque as high as $\Delta T_{cog} = 11.1\%$.

TABLE VI
2D VERSUS 3D FEA TORQUE CALCULATIONS AT n_r.

PMVG	$G_r = 5$	$G_r = 8$	$G_r = 11$
2D T_g (Nm)	122.1	124.9	122.9
3D T_g (Nm)	125.6	123.6	120.6

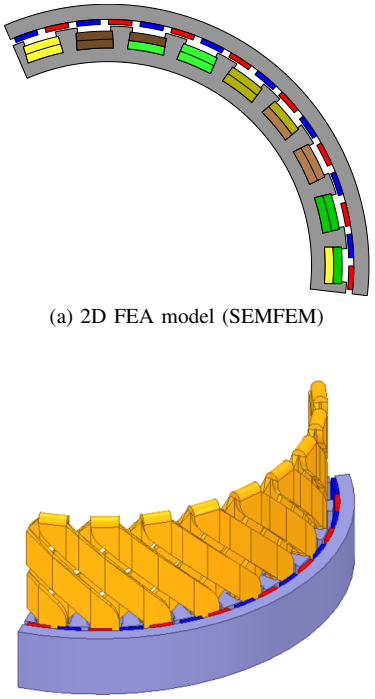

(a) 2D FEA model (SEMFEM)

(b) 3D FEA model (ANSYS Maxwell)

Fig. 10. Partial 2D and 3D FEA models for the $G_r = 8$ PMVG in Table IV.

D. FEA Validation

All of the designs in the optimisation were done with 2D static FEA. To verify the design results, the selected PMVGs in Table IV are also solved with 3D FEA models. The partial 2D and 3D FEA models for the PMVG with $G_r = 8$, are shown in Fig. 10(a) and (b) respectively. For the 2D FEA, an in-house package, SEMFEM, is used. For the 3D FEA, the commercial package, ANSYS Maxwell, is used. The generated torque results at the rated operating point, n_r, are summarised and compared in Table VI. The results show very good correlation between the 2D and 3D FEA solutions and verify that the obtained results are accurate. More specifically, the comparison in Table VI indicates that the end-winding calculations and the accounting for end-effects, done in the 2D FEA, are sufficient.

E. Discussion on Future Prototyping

One foreseeable issue with prototyping, is that the end-winding lengths of the PMVG's overlapping coils are extremely long. The end-windings are shown in Fig. 10(b). For this application it is desired that the generator be as volumetrically compact as possible, and therefore, the long end-windings are not considered to be practical. Thus, it would

Authorized licensed use limited to: University of Stellenbosch. Downloaded on June 16,2021 at 11:45:02 UTC from IEEE Xplore. Restrictions apply.

be favourable to also consider the split-tooth topology PMVG with non-overlapping windings for this application in future work.

VI. Conclusion

In this paper, it is proposed that PMVGs be used in a small-scale uncontrolled passive wind generator system for rural stand-alone power generation. The aim of the investigation is to determine whether the proposal is feasible, seeing as PMVGs have not previously been considered for this application. The following main conclusions are drawn from the investigation:

In terms of the wind generator's power matching with the wind turbine, it is found that PMVGs are excellently suited for passive wind generator systems. The inherently high internal reactance of PMVGs, which is typically considered to be its main drawback, is found to be advantageous for this application. As a result, all of the PMVG designs, that are uncontrolled and operate at a unity displacement power factor, naturally achieve the desired power matching with the wind turbine.

The PMVG with a magnetic gearing ratio of $G_{\mathrm{r}} = 8$ is very attractive for this application, because of its torque producing capability and torque quality. However, the PMVG machine selection is one aspect that should be carefully considered for this application. For instance, it is found that PMVGs with $G_{\mathrm{r}} = 5$ should be avoided due to high cogging torque and undesired torque ripple.

Although there is no direct comparison done in this paper, the optimisation results indicate that using PMVGs for this application might be more cost effective than using conventional surface-mounted PMSGs [9] and that PMVGs can have superior torque quality. Furthermore, PMSGs often require an additional external inductance for good power matching with the wind turbine [9], whereas PMVGs do not. Therefore, the initial design results presented in this paper are indicative that PMVGs might be superior to PMSGs for this application.

The main concern, is the undesired long end-winding lengths of the PMVG's overlapping windings. For future work, the split-tooth PMVG topology with non-overlapping windings should also be considered and compared to the conventional PMVG with overlapping windings.

References

[1] B. Kim, "Design method of a direct-drive permanent magnet vernier generator for a wind turbine system," *IEEE Transactions on Industry Applications*, vol. 55, no. 5, pp. 4665–4675, 2019.

[2] D. K. K. Padinharu, G. J. Li, Z. Q. Zhu, R. Clark, A. S. Thomas, and Z. Azar, "System-level investigation of multi-MW direct-drive wind power PM vernier generators," *IEEE Access*, vol. 8, pp. 191 433–191 446, 2020.

[3] F. Wu and A. M. El-Refaie, "Permanent magnet vernier machine: a review," *IET Electric Power Applications*, vol. 13, no. 2, pp. 127–137, 2019.

[4] D. Li, R. Qu, and T. A. Lipo, "High-power-factor vernier permanent-magnet machines," *IEEE Transactions on Industry Applications*, vol. 50, no. 6, pp. 3664–3674, 2014.

[5] W. Li, T. W. Ching, and K. T. Chau, "A hybrid-excited vernier permanent magnet machine using homopolar topology," *IEEE Transactions on Magnetics*, vol. 53, no. 11, pp. 1–7, 2017.

[6] E. I. Baring-Gould, R. W. Preus, R. Wills, D. Davis, K. R. Jackson, and S. Dana, "Competitiveness improvement project informational workshop," National Renewable Energy Lab.(NREL), Golden, CO (United States), Tech. Rep., 2020.

[7] M. Arifujjaman, M. T. Iqbal, and J. E. Quaicoe, "Reliability analysis of grid connected small wind turbine power electronics," *Applied Energy*, vol. 86, no. 9, pp. 1617 – 1623, 2009.

[8] P. M. Tlali, R. Wang, S. Gerber, C. D. Botha, and M. J. Kamper, "Design and performance comparison of vernier and conventional PM synchronous wind generators," *IEEE Transactions on Industry Applications*, vol. 56, no. 3, pp. 2570–2579, 2020.

[9] C. J. J. Labuschagne and M. J. Kamper, "Evaluation of PM rotor topologies for impedance matching of small-scale passive dc-connected wind generator systems," in *2020 International Conference on Electrical Machines (ICEM)*, vol. 1, 2020, pp. 1896–1902.

[10] N. Mohan, T. M. Undeland, and W. P. Robbins, *Power Electronics: converters, applications, and design*. John Wiley & Sons, 2003.

[11] A. Toba and T. A. Lipo, "Generic torque-maximizing design methodology of surface permanent-magnet vernier machine," *IEEE Transactions on Industry Applications*, vol. 36, no. 6, pp. 1539–1546, 2000.

[12] K. Deb, S. Agrawal, A. Pratap, and T. Meyarivan, "A fast elitist non-dominated sorting genetic algorithm for multi-objective optimization: NSGA-II," in *International conference on parallel problem solving from nature*. Springer, 2000, pp. 849–858.

[13] C. J. J. Labuschagne and M. J. Kamper, "Wind generator impedance matching in small-scale passive wind energy systems," *IEEE Access*, vol. 9, pp. 22 558–22 568, 2021.

[14] D. K. Kana Padinharu, G. J. Li, Z. Q. Zhu, Z. Azar, R. Clark, and A. Thomas, "Effect of airgap length on electromagnetic performance of surface mounted permanent magnet vemier machine," in *2020 International Conference on Electrical Machines (ICEM)*, vol. 1, 2020, pp. 1882–1888.

[15] Z. Q. Zhu and D. Howe, "Influence of design parameters on cogging torque in permanent magnet machines," *IEEE Transactions on Energy Conversion*, vol. 15, no. 4, pp. 407–412, 2000.

Authorized licensed use limited to: University of Stellenbosch. Downloaded on June 16,2021 at 11:45:02 UTC from IEEE Xplore. Restrictions apply.